Nuclear Instruments and Methods in Physics Research B 374 (2016) 45–50

Contents lists available at ScienceDirect

Nuclear Instruments and Methods in Physics Research B

journal homepage: www.elsevier.com/locate/nimb

Anomalous dispersion and band gap reduction in UO_{2+x} and its possible coupling to the coherent polaronic quantum state

Steven D. Conradson [a,*], David A. Andersson [b], Paul S. Bagus [c], Kevin S. Boland [b], Joseph A. Bradley [b], Darrin D. Byler [b], David L. Clark [b], Dylan R. Conradson [b], Francisco J. Espinosa-Faller [d], Juan S. Lezama Pacheco [b], Mary B. Martucci [b], Dennis Nordlund [f], Gerald T. Seidler [e], James A. Valdez [b]

[a] Synchrotron Soleil, Saint-Aubin BP-48, 91192, France
[b] Los Alamos National Laboratory, Los Alamos, NM 87545, United States
[c] University of North Texas, Denton, TX 76203, United States
[d] Universidad Marista de Merida, Merida, Yucatan 97300, Mexico
[e] University of Washington, Seattle, WA 98195, United States
[f] SLAC National Accelerator Laboratory, Menlo Park, CA 94025, United States

ARTICLE INFO

Article history:
Received 30 September 2015
Accepted 31 October 2015
Available online 11 December 2015

Keywords:
UO_{2+x}
Covalency
Coherence
Band structure
XAS

ABSTRACT

Hypervalent UO_2, $UO_{2(+x)}$ formed by both addition of excess O and photoexcitation, exhibits a number of unusual or often unique properties that point to it hosting a polaronic Bose–Einstein(-Mott) condensate. A more thorough analysis of the O X-ray absorption spectra of UO_2, U_4O_9, and U_3O_7 shows that the anomalous increase in the width of the spectral features assigned to predominantly U 5*f* and 6*d* final states that points to increased dispersion of these bands occurs on the low energy side corresponding to the upper edge of the gap bordered by the conduction or upper Hubbard band. The closing of the gap by 1.5 eV is more than twice as much as predicted by calculations, consistent with the dynamical polaron found by structural measurements. In addition to fostering the excitation that is the proposed mechanism for the coherence, the likely mirroring of this effect on the occupied, valence side of the gap below the Fermi level points to increased complexity of the electronic structure that could be associated with the Fermi topology of BEC–BCS crossover and two band superconductivity.

1. Introduction

As the origin of many of the interesting properties of matter, covalency is as important as it is awkward to define [1]. In classic real space physics, if the role of quantum mechanics is to define the distribution of electrons but the forces are electrostatic, then covalency is the accumulation of electron density between the nuclei that renders the overall force between the atom pair attractive. An important factor is therefore the spatial extent of the original atomic orbitals since their overlap determines the shared volume available for building up the charge. The concept of covalency is more easily depicted in momentum space as the shifts in the energy levels of the molecular orbitals from their parent atomic states in molecules and the dispersion of the bands in condensed systems. The structures of transition metals possessing localized electrons in flat bands tend to be defined by the longer range magnetic interactions of the isolated spins. In contrast, delocalized, itinerant electrons can interact directly to give bands with large dispersions, with bulk properties that result from these bonds. Elements in the crossover region are the ones that display polymorphism, complicated magnetism, chemically reactive electronic states, and other manifestations of correlated electrons.

The rare earth elements, whose frontier 4*f* orbitals are confined to the core of the atom, and the heavier actinides whose 5*f* orbitals are similarly constrained therefore for the most part behave in predictable and relatively unexciting ways. The lighter actinides are, however, the opposite, with one example being the radical change in atomic radius at plutonium [2,3]. Residing at the crossover between spatially extended and localized 5*f* orbitals, it is the most complex element in the periodic table with six solid phases encompassing monoclinic to fcc symmetries, two of which exhibit negative thermal expansion coefficients, that span a 22% range of densities before it melts from the bcc ε phase into a higher density liquid at a relatively modest 912.5 K. In addition to this evidence for the ambiguity in the ability of the 5*f* states to overlap, it has also recently been shown that the absence of the predicted magnetism

* Corresponding author.

http://dx.doi.org/10.1016/j.nimb.2015.10.073
0168-583X/

in Pu is because the temporal fluctuations that create hybridized or mixed electronic states in dynamical mean field theory appear to have physical significance, scrambling the spins faster than they can collectively orient [4]. It would not be surprising if these two phenomena, one in time and one in space, are coupled. This pattern of diversity is also displayed in their chemistry. Pm-Am exhibit an usually large number of valences in their chemical compounds that are correlated with a radical change in bonding and symmetry from spherical and highly ionic in their (III) and (IV) states to the highly oblate (trans di-) oxo moiety with the ultra short, triply bonded oxo ion for (V)–(VII), or a tetraoxo configuration under certain conditions [1,5].

Analogous to Pu metal, the most complicated binary metal oxide phase diagram may be that for U [6,7] where there is not even consensus whether the number of distinct compounds between $UO_{1.5}$ and UO_3 is greater than 20 [8] or not [9]. It divides into two regions. Below $UO_{2.33-2.5}$ the structures are strictly or approximately cubic. At temperatures below those where rapid O diffusion eliminates crystallographic disorder there are two mixed valence compounds that are single phase in diffraction, U_4O_9 and U_3O_7, although the multiplicity of their extended superlattices has prevented their structures from being completely solved [10–14]. Even in this ionic region, however, there are indications of more complexity, such as superionic conductivity of UO_{2+x} and the aggregation of the adventitious O in UO_{2+x} so that it is better described as UO_2:U_4O_9 and U_4O_9:U_3O_7 mixtures [10,15,16]. At higher O:U ratios the structures are layered because of the propensity of U(V) and (VI) to form the trans dioxo species. Another unusual or even unique anomaly is the loss of the normal correlation between valence and geometry/bond length in the higher oxides. In molecular or coordination compounds the U—O bonding patterns are quite rigid with the distances falling into ranges of only a few hundredths of an Å, [5] with the only suggestion of flexibility being a small expansion of the U-oxo bond that is coupled to greatly increased lability in hydroxide complexes [17]. However, in the solid state the α phase of UO_3 is highly oblate with an extremely short reported 1.64 Å U-oxo distance, [18] whereas the δ phase prepared by a slightly different procedure places the U ions in fully octahedral sites with U—O equals 2.08 Å, [19] with the intermediate phases giving intermediate distances in less distorted sites [20,21]. If the ternary uranates are included, [22–25] U(VI) exhibits essentially a continuous range of U—O bond lengths from 1.64 to 2.45 Å and longer. U(V) displays a continuous range of U—O distances from 1.9 to 2.7 Å in a single compound, U_2O_5. This behavior implies an exceptionally flat U—O potential for the higher valences that is highly susceptible to small changes in other factors influencing the structure and that can shift quite easily in response to such factors. It also implies a large degree of what would most likely be termed covalency; hard spherical ions do not change their conformations because of interactions with their neighbors. The shortness of the U-oxo bond points to a predilection for covalency that could potentially be distributed to other bonds if it is diminished in that one.

These properties of U(V) and (VI) that stabilize them in layered structures and the way they combine with the much less covalent U(IV) ions [26] with their cubic or spherical geometries underlie the special flexibility of the (1 1 1) planes in UO_2 [27]. Not only do dislocation loops form along them, [28] but their easy [1 1 1] expansion also causes substitutional cations that prefer octahedral environments, e.g., Cr^{3+}, to cluster along them as well. This behavior establishes the environment that promotes the dynamical polaron in fluorite structured, chemically or photodoped $UO_{2(+x)}$ [29,30]. The 2 U(V) ↔ U(IV) + U(VI) disproportionation excitation of these polarons would occur easily via the transfer of O ions between their buckled-apical positions for fluorite and planar-apical positions for layered, triggered by a [1 1 1] type acoustic phonon that causes the separation of the (1 1 1) U planes to oscillate. The synchronization of this internal reaction throughout the U_4O_9-type domain formed by the aggregation of the adventitious O or photoinduced charges then gives the coherence that defines the polaronic Bose–Einstein(-Mott) condensate. We have previously reported the O XAS of UO_{2+x} that demonstrated a significant enhancement of the widths of the U 5*f* states in the upper Hubbard band (UHB, the conduction band) that is opposed to the trend of narrower spectral features with increasing charge [29] that we attributed to the mixing of the electronic states and increased dispersion that occurs with a dynamical polaron [31]. We now examine these results in greater detail to show that this increased dispersion specifically reduces the lower boundary of the UHB. This substantial reduction of the gap energy and the increased DOS within the UO_2 gap would then facilitate the excitation that results in the condensate formation [30]. In addition, it is likely that the cause of this effect acts on additional U 5*f* states so that it is mirrored in the lower Hubbard band (LHB, valence band). This would be of significant interest because much recent work on BEC–Barden–Cooper–Schrieffer (BCS) superconducting condensate crossover in mixed valence metal oxide and chalcogenide exotic superconductors is focused on the character of these bands closest to the Fermi level [32] and its implications for two band superconductivity [33–39].

2. Experimental and calculation methods

Samples were prepared and NIXS and XAS experiments were performed as previously described, [29,40–42] as were the calculations [43].

3. Results and discussion

3.1. O XAS of standards and UO_2

The O XAS of U-oxides [44–49] and even the oxo group of uranyl-containing molecules that are coordination complexes of U(VI) [50] consist of two principal features (Fig. 1). There is consensus not only for UO_2 but for all of them that, in agreement with theory, the lower energy feature around 530–535 eV originates in transitions to unoccupied states of the upper Hubbard band (UHB) that are predominantly U 5*f* in character and the higher energy feature around 537–543 eV in transitions to unoccupied states that are predominantly U 6*f*. This is true not only for UO_2 where the U is in a cubic site and the O surrounded by a tetrahedron of U, but also for layered compounds such as U_3O_8 with relatively long U—O_{oxo} bonds and α UO_3 with its extremely short one and even the oxo O ion in $Cs_2UO_2Cl_4$. The pattern is the result of the symmetry relationship between cubic and octahedral geometries where the latter results from locating a neighbor atom in the center of each of the six square that constitute the cube's sides whose corners are the eight vertices. It is also because the shift in energy between the different types of O, terminal oxo, symmetrically bridging oxo, asymmetrically bridging oxo, and planar O with varying coordination numbers and bond lengths is less than 1 eV. The increase in the width of the peaks in the layered oxides with their multiple O species relative to that of the single type of O in the uranyl tetrachloride is therefore not excessive. The spectral pattern is therefore preserved across all of these species because the differences in energies for the different O and U species are much smaller than their U 5*f*-5*d* separations that are relatively insensitive to the speciation and geometry [48].

The exception to this assignment is the small shoulder on the leading edge of the first peak. This was not assigned for $Cs_2UO_2Cl_4$ despite a very thorough set of experiments that utilized

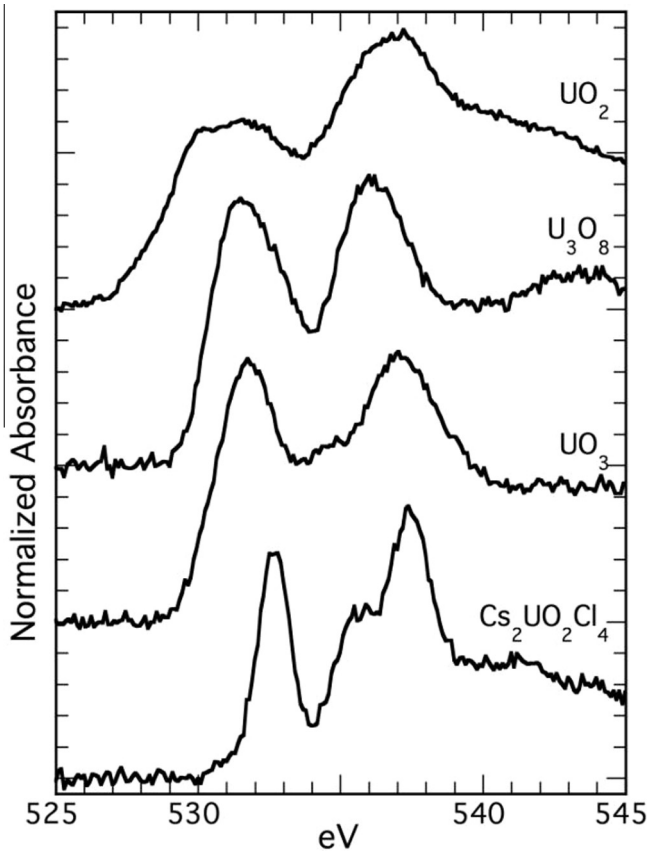

Fig. 1. O XAS fluorescence yield spectra of indicated compounds (UO_3 is in the uranyl containing α phase) with edge jumps normalized to unity. These are not calibrated.

polarization dependence of single crystals and emission spectra [50]. Curve-fits show that it is necessary for all of these spectra even when the change in slope is not apparent. Because the analysis of the tetrachloride utilized the transitions to the lowest energy unoccupied states it is difficult to explain. One possibility is a multi-electron transition.

For UO_2, the peaks or shoulders signifying peaks at around 530–531, 532, 534, 537, 539, 540, 542, and 545 eV are relatively consistent in their energies and sufficiently consistent in their relative amplitudes so that the overall shapes are similar [26,44–47,49]. The precise intensities and shapes of these two features, however, vary between samples (Fig. 2) even when their impurity levels are at or below the 100 ppm range. The changes in relative amplitudes result in motions of some of the features, including the leading edge of the first peak around 531 eV and the valley at 535–536 eV. The spectral features are therefore affected by even the small amounts of disorder that vary between different preparations, which in an XAS measurement will be exacerbated by the surface quality. This comparison, then, provides a measure of the level of reproducibility to expect in evaluating the spectra from different compounds.

Within this level of uncertainty, it is apparent that these two spectral features for UO_2 are significantly and consistently wider than those from the other non-fluorite compounds. Both of them consist of multiple peaks, causing their flatness across the tops. Calculations indicate that this is an effect of spin–orbit coupling [49,51–53] that causes multiplet splitting in the spectra. The reduction in such splitting as the valence increases and the number of electrons residing in these states decreases therefore explains the observed narrowing of the spectral features.

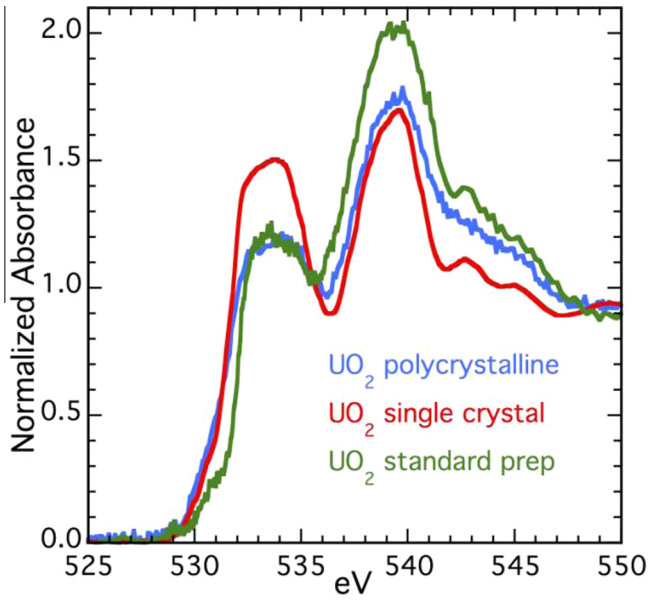

Fig. 2. O XAS fluorescence yield measurements of UO_2 from a single crystal, which will have the highest surface quality and impurity level, polycrystalline material prepared from recrystallized UO_2O_2 that will have the lowest impurity concentrations, and from commercially available high purity UO_2 that is reduced to $UO_{2.00}$ by standard procedures.

3.2. O XAS and NIXS of UO_{2+x}

In addition to variations because of surface quality, XAS spectra at these energies are affected by self-absorption because the samples are fully opaque to the X-rays. Self-absorption causes a flattening of the spectra around the average absorption, increasing the amplitudes of features below this average proportionate to the amount by which they are less than this average, and reducing the amplitudes of features above the average absorption in the same way. Both of these problems that distort the spectra are solved by using Non-resonant Inelastic X-ray Scattering (NIXS) with a high energy ($\sim$10 keV) beam that penetrates deeply into the sample [40,41]. The NIXS spectra can therefore confirm the features constituting the more conventionally measured but surface sensitive XAS and also give the correct amplitudes, albeit with much greater noise levels because of the weakness of the NIXS signal. The comparison (Fig. 3) of the NIXS and XAS using this information validates the measured spectra.

This verification is crucial because the spectra of these mixed valence compounds do not adhere to the pattern exhibited by the other U compounds (Figs. 1 and 3). For U_3O_7 the U 5*f* manifold is greatly reduced. For U_4O_9 there is no distinct feature separated by an equally distinct valley from the principal one at higher energy, all features are suppressed so that after the initial abrupt rise the spectrum is almost featureless – or contains a number of very small features – until it rises somewhat more steeply to a low peak in the U 6*d* region.

Because of the self-absorption issues the positions and widths of the features are best obtained via the NIXS spectra. The differences in amplitude, energy, and the presence or absence of features are apparent when the spectra are overlaid (Fig. 4). Also obvious is that the U_4O_9 spectrum is not an average of the UO_2 and U_3O_7 endpoints [29] despite the supposition that it contains the same defects and therefore O environments whose larger number in U_3O_7 are simply organized differently.

The noise level of the NIXS causes difficulties in determining the energies of the features, a problem that is ameliorated by taking

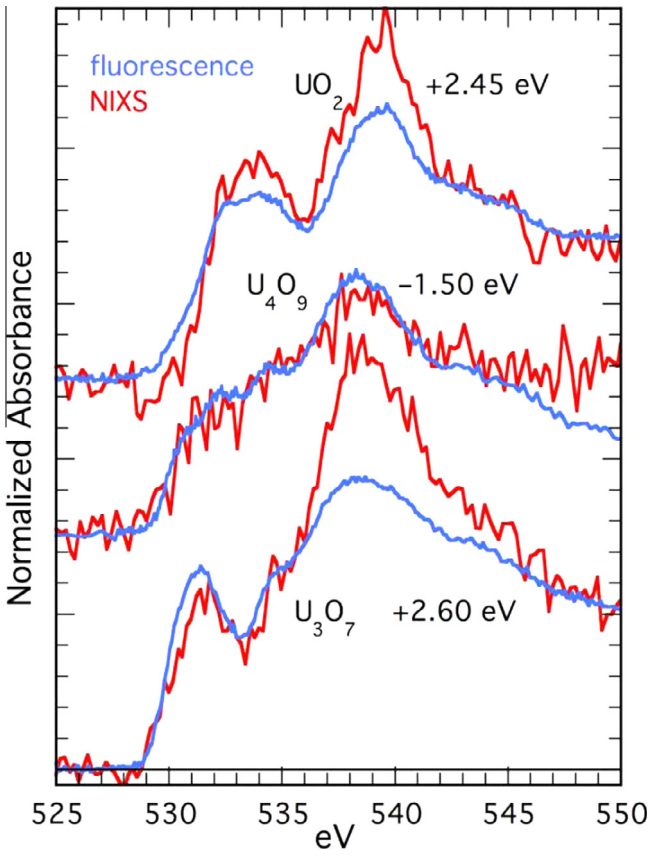

Fig. 3. Fluorescence yield and NIXS spectra of UO_{2+x} compounds. Numbers are the shift of the FY data to match the NIXS whose energies are set by the difference from the excitation line.

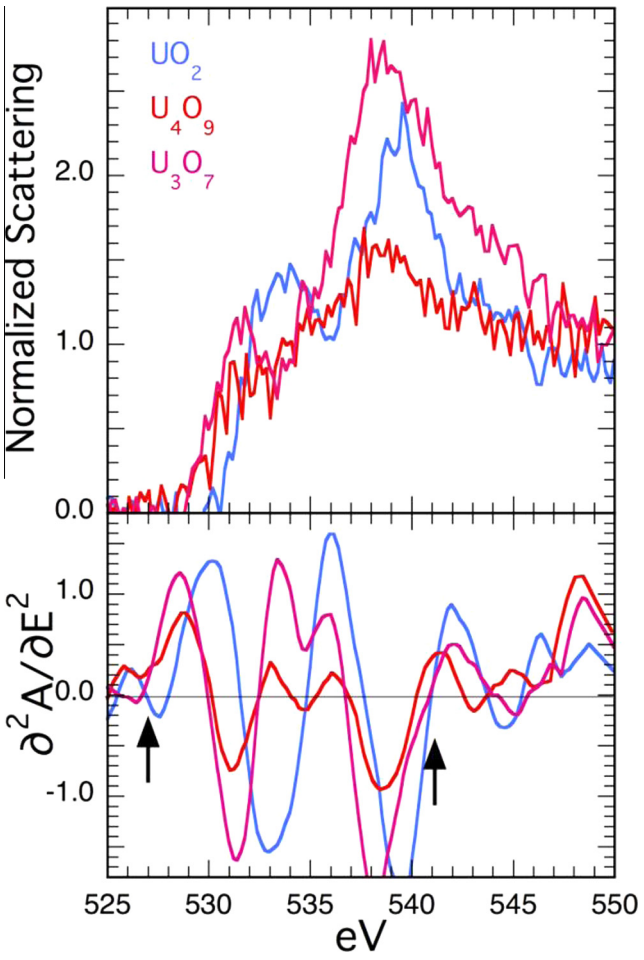

Fig. 4. NIXS spectra of UO_{2+x} compounds, absorbance and second derivatives. The arrows indicate the locations of the inflection points for the initial edge jump that would be the initial energy for the UHB and the limit of the large feature assigned to U 6*d* final states and therefore mark the boundaries of the U DOS.

the derivatives that also finds the energies of the features of interest more accurately. In this case the issue is not the increase in the dispersion and total width of the DOS with doping that has been described previously [29] but more specifically the effects on the gap. The energies of the inflection points of the initial absorption increase are 531.5 for UO_2, 530.1 for U_4O_9, and 529.9 for U_3O_7, giving shifts of −1.4 and −1.6 eV for the O-doped compounds. In contrast, the values for the inflection point on the far side of the 538–539 eV peak are, respectively, 541.0, 540.3, and 540.9 eV. The shift for U_3O_7 is only −0.1 eV, which is in the uncertainty level. For U_4O_9 it is −0.7 eV. This would reduce the overall increase in the dispersion of the U DOS for this compound, but given the flatness of the spectrum because of the low amplitude of this peak and the high noise level the uncertainty is higher. We point out that the peaks of this feature for both doped compounds coincide, making it likely that the U 6*d* bands of U_4O_9 and U_3O_7 have similar overall energies. It is therefore notable that the increased dispersion of overall U DOS occurs as shifts to lower energy. To the extent that the principal peak reflects the U 6*d* states its increased width relative to that for UO_2 indicates that both these and 5*f* states are affected.

3.3. Comparison with calculations

The question of whether the broadening of the DOS to lower energies is expected or instead indicates an unusual phenomenon such as the condensate is addressed by DFT+U calculations [43] using the neutron-scattering type structure [10,13,54] that retains the fluorite lattice and incorporates the adventitious O into the vacant cubic sites concomitant with the displacement of some number of adjacent original O ions into neighboring sites. These calculations show (Fig. 5) the decrease in energy of the boundary

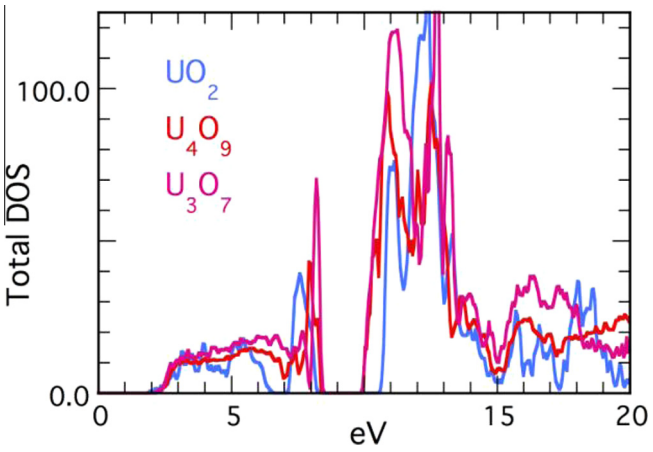

Fig. 5. DFT+U calculations of the total density of states for the normal and doped compounds.

and lowest energy peaks of the UHB as well as the shift of the DOS in the U 6*d* region to lower energy on doping and the reduced amplitude for U_4O_9 relative to U_3O_7. However, the reduction in the energy of the UHB edge is only half or somewhat less than half of the experimental value, and the calculation also fails to find the reduction or loss of the separation between the 5*f* and 6*d* states

that is seen in the spectra. Thus, instead of the −0.6 eV shift of the UHB edge with doping, with the overall gap shrinking by ~0.9 eV to reduce it from around 2.5 eV (somewhat larger than the experimental number of ~2.1 eV) to around 1.6 eV, the measurements show a shift of the initial absorption increase in the doped compounds relative to UO_2 of around −1.5 eV. Modeling has demonstrated that the energies of the local electronic states associated with dynamic polarons bend, with the deviations from a horizontal line increasing in tandem with the electron–phonon coupling constant. Avoided crossings can therefore actually change the state that occurs at the band edge. The energy differences between the states are also affected, with some increasing but other decreasing to give a small amount of absorption through the IR region down to almost zero energy. The dynamics that has been identified from the structural measurements and is intrinsic to the condensate and related phenomena can thus be a possible contributor or even cause of this large reduction in the UHB edge.

1.5 eV begins to approach the closing of the gap. This will be especially true if the lowering of the UHB is mirrored by a concomitant increase in the upper edge of the LHB that occurs in the calculations, which might be characterized by RIXS [55]. Such a process would be expected if the energy shifts in the levels associated with – using the analogy with molecules – antibonding states move in the opposite direction as those in the LBH that are involved in bonding. This correlation of the states that is the definition of covalency is a process for increasing the dispersion of the bands, as happens when O is added to UO_2 to give the mixed valence compounds. A reduction in the energy across the gap is consistent with the proposed mechanism involving a flat U—O pair potential and a facile excitation between the cubic U(V) ground state and the layered U(VI) excited state [29,30]. Although U(VI) was not detected in high resolution or RIXS studies, [55,56] insofar as the structural chemistry of U-oxides required this valence for the short distances that have been identified by XAFS [57] it is possible that the improvement in energy resolution increases the time domain via the uncertainty principle, confining the experiment to the ground state. In addition, as previously stated, this region is of interest because this upper edge of the valence band is where not only BEC but also BCS states will occur, stimulated or at enhanced by the same dispersion, avoided crossings, and similar covalency-related correlated phenomena. This multiplicity of bands at the Fermi level is the basis for the complicated Fermi topology that is coupled to BEC–BCS crossover [32] and two-band exchange as the origin of pseudogap states and exotic superconductivity [33–39] and would therefore place $UO_{2(+x)}$ within this class of materials, albeit at an extreme position.

Acknowledgements

This work was supported at Los Alamos by the Division of Chemical Sciences, Geosciences, and Biosciences, Office of Basic Energy Sciences, U.S. DOE, under the Heavy Element Chemistry Program at LANL, a Glenn T. Seaborg Institute graduate fellowship (J.B.), and the Los Alamos Laboratory Directed Research and Development Program. Portions of this research were carried out at the Stanford Synchrotron Radiation Laboratory (SSRL) and the Advanced Photon Source (APS), both of which are national user facilities supported by the U.S. Department of Energy, Office of Basic Energy Sciences. Los Alamos National Laboratory is operated by Los Alamos National Security, LLC, for the National Nuclear Security Administration of U.S. Department of Energy under Contract DE-AC52-06NA25396. PNC/XOR facilities at the Advanced Photon Source, and research at these facilities, are supported by the U.S. Department of Energy-Basic Energy Sciences, a Major Resources support grant from NSERC, the University of Washington, Simon Fraser University and the Advanced Photon Source. Use of the Advanced Photon Source is also supported by the U.S. Department of Energy, Office of Science, Office of Basic Energy Sciences, under Contract DE-AC02-06CH11357. PSB acknowledges the Geosciences Research Program, Office of Basic Energy Sciences, DOE.

References

[1] M.L. Neidig, D.L. Clark, R.L. Martin, Covalency in f-element complexes, Coord. Chem. Rev. 257 (2013) 394–406.
[2] S.S. Hecker, The magic of plutonium: 5f electrons and phase instability, Metall. Mater. Trans. A 35A (2004) 2207–2222.
[3] S.S. Hecker, D.R. Harbur, T.G. Zocco, Phase stability and phase transformations in Pu–Ga alloys, Prog. Mater. Sci. 49 (2004) 429–485.
[4] M. Janoschek et al., The valence-fluctuating ground state of plutonium, Sci. Adv. 1 (2015) e1500188.
[5] K.E. Knope, L. Soderholm, Solution and solid-state structural chemistry of actinide hydrates and their hydrolysis and condensation products, Chem. Rev. 113 (2013) 944–994.
[6] R.G. Haire, L. Eyring, in: K.A. Gschneidner Jr., L. Eyring, G.R. Choppin, G.H. Lander (Eds.), Handbook on the Physics and Chemistry of the Rare Earths, Elsevier Science, B.V., 1994, pp. 413–505.
[7] W.T. Thompson et al., Thermodynamic treatment of uranium dioxide based nuclear fuel, Int. J. Mater. Res. 98 (2007) 1004–1011.
[8] G.C. Allen, N.R. Holmes, A mechanism for the UO_2 to alpha-U_3O_8 phase-transformation, J. Nucl. Mater. 223 (1995) 231–237.
[9] G.C. Allen, P.A. Tempest, Ordered defects in the oxides of uranium, Proc. R. Soc. London Ser. A 406 (1986) 325–344.
[10] B.T.M. Willis, Defect structure of hyper-stoichiometric uranium-dioxide, Acta Crystallogr. A 34 (1978) 88–90.
[11] D.J.M. Bevan, I.E. Grey, B.T.M. Willis, The crystal-structure of beta-U_4O_{9-y}, J. Solid State Chem. 61 (1986) 1–7.
[12] R.I. Cooper, B.T.M. Willis, Refinement of the structure of beta-U_4O_9, Acta Crystallogr. A 60 (2004) 322–325.
[13] F. Garrido, A.C. Hannon, R.M. Ibberson, L. Nowicki, B.T.M. Willis, Neutron diffraction studies of U_4O_9: comparison with EXAFS results, Inorg. Chem. 45 (2006) 8408–8413.
[14] L. Desgranges, G. Badinozzi, D. Simeone, H.E. Fischer, Refinement of the alpha-U_4O_9 crystalline structure: new insight into the $U_4O_9 \rightarrow U_3O_8$ transformation, Inorg. Chem. 50 (2011) 6146–6151.
[15] F. Garrido, R.M. Ibberson, L. Nowicki, B.T.M. Willis, Cuboctahedral oxygen clusters in U_3O_7, J. Nucl. Mater. 322 (2003) 87–89.
[16] H.Y. Geng et al., Point defects and clustering in uranium dioxide by LSDA+U calculations, Phys. Rev. B 77 (2008). 104120/104121-104116.
[17] D.L. Clark et al., Chemical speciation of the uranyl ion under highly alkaline conditions. Synthesis, structures, and oxo ligand exchange dynamics, Inorg. Chem. 38 (1999) 1456–1466.
[18] C. Greaves, B.E.F. Fender, Structure of alpha-UO_3 by neutron and electron-diffraction, Acta Crystallogr. B 28 (1972) 3609–3614.
[19] M.T. Weller, P.G. Dickens, D.J. Penny, The Structure of delta-UO_3, Polyhedron 7 (1988) 243–244.
[20] R. Engmann, P.M.D. Wolff, Crystal structure of gamma-UO_3, Acta Crystallogr. 16 (1963) 993–996.
[21] P.C. Debets, Structure of beta-UO_3, Acta Crystallogr. 21 (1966) 589–593.
[22] R.B. King, Some aspects of structure and bonding in binary and ternary uranium(VI) oxides, Chem. Mater. 14 (2002) 3628–3635.
[23] H.M. Rietveld, Crystal structure of some alkaline earth metal uranates of type M_3UO_6, Acta Crystallogr. 20 (1966) 508–513.
[24] P.G. Dickens, A.V. Powell, Powder neutron-diffraction study of potassium uranate(V), KUO_3, J. Mater. Chem. 1 (1991) 137–138.
[25] S. Van den Berghe et al., The local uranium environment in cesium rranates: a combined XPS, XAS, XRD, and neutron diffraction analysis, J. Solid State Chem. 166 (2002) 320–329.
[26] J.G. Tobin et al., Covalency in oxidized uranium, Phys. Rev. B 92 (2015).
[27] L. Desgranges, P. Simon, P. Martin, G. Guimbretiere, G. Baldinozzi, What can we learn from Raman spectroscopy on irradiation-induced defects in UO_2?, JOM 66 (2014) 2546–2552
[28] L.F. He et al., In situ TEM observation of dislocation evolution in polycrystalline UO_2, JOM 66 (2014) 2553–2561.
[29] S.D. Conradson et al., Possible Bose condensate behavior in a quantum phase originating in a collective excitation in the chemically and optically doped Mott–Hubbard system, $UO_{2(+x)}$, Phys. Rev. B 88 (2013) 115135.
[30] S.D. Conradson et al., Possible demonstration of a polaronic Bose–Einstein(-Mott) condensate in $UO_{2(+x)}$ by ultrafast THz spectroscopy and microwave dissipation, Sci. Rep. 5 (2015) 15278.
[31] M.I. Salkola, A.R. Bishop, S.A. Trugman, J.M. Deleon, Correlation-function analysis of nonlinear and nonadiabatic systems-polaron tunneling, Phys. Rev. B 51 (1995) 8878–8891.
[32] K. Okazaki et al., Superconductivity in an electron band just above the Fermi level: possible route to BCS–BEC superconductivity, Sci. Rep. 4 (2014) 4109.
[33] A. Bianconi, The instability close to the 2d generalized Wigner polaron crystal density-a possible pairing mechanism indicated by a key experiment, Physica C 235 (1994) 269–272.

[34] A. Bianconi, Feshbach shape resonance in multiband superconductivity in heterostructures, J. Supercond. 18 (2005) 625–636.
[35] M. Fratini, N. Poccia, A. Bianconi, International symposium on lattice effects in cuprate high temperature superconductors, in: H. Oyanagi, H. Eisaki (Eds.), Journal of Physics Conference Series 012036, vol. 108, 2008.
[36] A. Vittorini-Orgeas, A. Bianconi, From majorana theory of atomic autoionization to feshbach resonances in high temperature superconductors, J. Supercond. Novel Magn. 22 (2009) 215–221.
[37] A. Bianconi, Shape resonances in superstripes, Nat. Phys. 9 (2013) 536–537.
[38] A. Bianconi, Shape resonances in multi-condensate granular superconductors formed by networks of nanoscale-striped puddles, in: 10th International Conference on Materials and Mechanisms of Superconductivity (M2s-X), vol. 449, 2013, p. 012002.
[39] A. Guidini, A. Perali, Band-edge BCS–BEC crossover in a two-band superconductor: physical properties and detection parameters, Supercond. Sci. Tech. 27 (2014) 124002.
[40] J.A. Bradley et al., Experimental and theoretical comparison of the O K-edge nonresonant inelastic X-ray scattering and X-ray absorption spectra of $NaReO_4$, J. Am. Chem. Soc. 132 (2010) 13914–13921.
[41] J.A. Bradley et al., Probing electronic correlations in actinide materials using multipolar transitions, Phys. Rev. B 81 (2010). 193104/193101-193104.
[42] S.A. Kozimor et al., Covalency trends in group IV metallocene dichlorides. Chlorine K-edge X-Ray absorption spectroscopy and time dependent-density functional theory, Inorg. Chem. 47 (2008) 5365–5371.
[43] D.A. Andersson, G. Baldinozzi, L. Desgranges, D.R. Conradson, S.D. Conradson, Density functional theory calculations of UO_2 oxidation: evolution of UO_{2+x}, U_4O_{9-y}, U_3O_7, and U_3O_8, Inorg. Chem. 52 (2013) 2769–2778.
[44] F. Jollet et al., The electronic structure of uranium dioxide: an oxygen K-edge X-Ray absorption study, J. Phys. Condens. Matter 9 (1997) 9393–9401.
[45] Z.Y. Wu et al., X-ray absorption at the oxygen K edge in cubic f oxides examined using a full multiple-scattering approach, J. Phys. Condens. Matter 11 (1999) 7185–7194.
[46] S.W. Yu et al., F-f origin of the insulating state in uranium dioxide: X-ray absorption experiments and first-principles calculations, Phys. Rev. B 83 (2011). 165102/165101-165108.
[47] M. Magnuson et al., Uranium oxides investigated by X-ray absorption and emission spectroscopies, Appl. Surf. Sci. 252 (2006) 5615–5618.
[48] X.-D. Wen et al., Electronic structure and O K-edge XAS spectroscopy of U_3O_8, J. Electron Spectrosc. Relat. Phenom. (2014) 81–87.
[49] J.G. Tobin et al., Oxidation and crystal field effects in uranium, Phys. Rev. B 92 (2015).
[50] R.G. Denning et al., Covalency in the uranyl ion: a polarized X-Ray spectroscopic study, J. Chem. Phys. 117 (2002) 8008–8020.
[51] J. Heyd, J.E. Peralta, G.E. Scuseria, R.L. Martin, Energy band gaps and lattice parameters evaluated with the Heyd–Scuseria–Ernzerhof screened hybrid functional, J. Chem. Phys. 123 (2005).
[52] X.-D. Wen et al., Effect of spin-orbit coupling on the actinide dioxides AnO_2 (An = Th, Pa, U, Np, Pu, and Am): a screened hybrid density functional study, J. Chem. Phys. 137 (2012) 154707.
[53] T. Vitova et al., Polarization dependent high energy resolution X-ray absorption study of dicesium uranyl tetrachloride, Inorg. Chem. 54 (2015) 174–182.
[54] A.D. Murray, B.T.M. Willis, A neutron-diffraction study of anion clusters in nonstoichiometric uranium-dioxide, J. Solid State Chem. 84 (1990) 52–57.
[55] K.O. Kvashnina, S.M. Butorin, P. Martin, P. Glatzel, Chemical state of complex uranium oxides, Phys. Rev. Lett. 111 (2013).
[56] T. Vitova et al., High energy resolution x-ray absorption spectroscopy study of uranium in varying valence states, Phys. Rev. B 82 (2010).
[57] S.D. Conradson et al., Local structure and charge distribution in the UO_2–U_4O_9 system, Inorg. Chem. 43 (2004) 6922–6935.